New erbium complexes emitting in infrared region based on oligothiophene and thiophenefluorene carboxylate

Silvia Destri[a],*, Mariacecilia Pasini[a], William Porzio[a], Fabio Rizzo[a,b,c],
Giovanna Dellepiane[b,c], Massimo Ottonelli[b,c], Gianfranco Musso[b,c],
Francesco Meinardi[d], Lucia Veltri[e]

[a]*Istituto per lo studio delle Macromolecole CNR, via E. Bassini 15, 20133 Milano, Italy*
[b]*Dipartimento di Chimica e Chimica Industriale Università di Genova, via Dodecaneso, 31 16146 Genova, Italy*
[c]*INSTM Via Benedetto Varchi n. 59, 50132 Firenze, Italy*
[d]*Dipartimento di Scienze dei Materiali, Università Milano Bicocca Via Cozzi 53, 20125 Milano, Italy*
[e]*Univ Calabria, Dipartimentodi Chimica, Arcavacata Di Rende I-87036, Italy*

Abstract

Lanthanide ions emitting in the near-infrared (NIR) region possess an intrinsically small molar absorption coefficient in the ultraviolet (UV)–vis–NIR spectrum, which is unfavourable for pumping efficiency. On the contrary, using organic lanthanide complexes it is possible to populate the excited state levels of the emitting ion through an efficient intramolecular energy transfer from the optically excited ligands, which act as light-harvesting antennae.

With the aim of studying and maximizing the transfer to lanthanide metals, we have synthesized oligothiophene and thiophenefluorene ligands bearing carboxylate clamps able to complex erbium and other lanthanide 3^+ ions. The complexes of {4′-(hydroxycarbonyl)methyl-[2,2′;5′,2′′]terthiophen-3′-yl}acetic acid and 9-(hydroxycarbonyl)-methyl-2,7-dithien-2-yl-[fluoren-9-yl-]acetic acid with Er^{3+} and different ancillary ligands have been prepared and their optical properties were carefully studied. Moreover, relaxation dynamics measurements have been carried out on all complexes in order to determine emission lifetimes, which result to be of the order of magnitude $2\,\mu s$. Quantum chemical calculations have been performed to explain optical absorption data in terms of different coordination types. The complexes containing phenanthroline/pyridine are modelled by adding to the dianion of the ligand one univalent/divalent counterion. The absorption spectra computed in this way are in close agreement with experiment, and the univalent → divalent theoretical wavelength shift goes in the right direction. The addition of a counterion has an even bigger effect on the triplet states, and hence on their matching with the emitting states of the ion.
© 2007 Elsevier B.V. All rights reserved.

1. Introduction

The possibility of exploiting the erbium (III) emission in planar optical amplifiers operating at $1.5\,\mu m$ has recently attracted much attention on the study of materials containing this ion [1,2]. Unfortunately, Er^{3+} has an intrinsically low miscibility in silica and, due to the forbidden character of its intra-4f transitions, has a small molar absorption coefficient in the ultraviolet (UV)–vis–near infrared (NIR) spectrum, which makes it unsuitable for pumping efficiency. On the contrary, organic chromophores usually have molar absorption coefficients 3–5 orders of magnitude larger [3,4]. Hence, population of emitting levels of Er^{3+} is best achieved by employing these chromophores as light-harvesting ligands that can sensitize the lanthanide ion via

*Corresponding author. Tel.: +390223699738; fax: +390270636400.
E-mail address: s.destri@ismac.cnr.it (S. Destri).

an intramolecular energy transfer process from their triplet states to metal excited states. Moreover, the complexes obtained in this way show good miscibility with plastic optical fibers (POF) enabling their use in amplification devices.

To achieve an efficient energy transfer, a matching is required between a triplet state of the organic sensitizer and the erbium levels corresponding to low-energy transitions such as $^4F_{7/2}$ (490 nm), $^2H_{11/2}$ (520 nm), $^4S_{3/2}$ (545 nm), $^4F_{9/2}$ (650 nm) or $^4I_{9/2}$ (800 nm). In this way, excitation wavelengths in the UV–vis spectrum may be reached, thus allowing use of relatively low-cost pumping sources. The energy transfer process can be realized either through direct coordination of a sensitizer multidentate molecule with a number of donor atoms or through coordination of a simple ligand covalently attached to a sensitizer molecule. Recently, also NIR emission originating from sensitizer functionalized ligand-based lanthanide (Er^{3+}, Nd^{3+}, and Yb^{3+}) complexes has been reported [5–8].

It is well known, however, that the NIR emission of Ln^{3+} ions can be strongly lowered by vibrational deactivation. The antenna, the ancillary ligands, the coordinated solvent (as well as moisture) usually contain high-energy oscillators such as O–H and C–H bonds (especially aromatic ones), which are able to quench the metal excited states nonradiatively, leading to decreased luminescence intensities and shorter excited-state lifetimes [9].

We have proposed {4′-(hydroxycarbonyl)methyl-[2,2′;5′,2″]terthiophen-3′-yl} acetic acid (hereafter referred to as **Lig. 1**, see Fig. 1) as a ligand that can satisfy the requirement of a low-energy excitation due mostly to the increased number of thiophene rings [10]. Afterwards, the possibility of synthesizing perfluorinated sexithiophene has been demonstrated [11]. The combination of these results allows to envisage the design and preparation of funzionalized oligomers absorbing at high wavelength and carrying the lower energy C–F oscillators in place of the C–H ones. Moreover, different ancillary ligands have been tested in order to overcome the well-known difficulty of crystallizing erbium complexes. We report here on the preparation and characterization of two complexes based on **Lig. 1** with either pyridine or phenanthroline as ancillary ligands. In addition, aiming to a progressive shift towards lower energy pumping sources, the oligomer 9-(hydroxycarbonyl)methyl-2,7-dithien-2-yl-[fluoren-9-yl-]acetic

acid (**Lig. 2**, see Fig. 1) has been prepared, in which a fluorene residue replaces a thiophene ring while maintaining the chelating functionality.

Electronic and Fourier transform infrared (FTIR) spectra strongly depend on the metal ion–carboxylate coordination. Hence quantum chemical calculations have been carried out in order to explain optical absorption data in terms of different coordinating types. We have studied the geometry, the electronic spectrum and the lowest triplet transitions of the neutral and doubly deprotonated forms of each isolated ligand. In the dianion case, the complexes containing phenanthroline/pyridine are modelled by adding one univalent/divalent counterion. The computed absorption spectra, as well as the univalent→divalent theoretical shift in the wavelength of the strongest absorption peak, are compared with experiment. The effect on triplet transitions of the addition of a counterion to the dianion has been also studied, and on these grounds predictions are made on the relative efficiency of the two ancillary ligands.

2. Experimental

All the procedures for complex preparation were carried out under nitrogen and using dry reagents to avoid the presence of water and oxygen, which can quench metal photoluminescence (PL).

2.1. Preparation of the acid Lig. 1

The procedure reported in Ref. [10] was slightly modified using a water: ethanol (1:1 v) reaction medium.

The resulting white yellowish acid was dried in vacuum for 24 h (yield 80%).

Mp 223–225 °C; FTIR (cm^{-1}) 3435(br, m), 3067(w), 1696 (s), 1469(m), 1420(m), 1207(m), 854(s). ^1H-NMR (270 MHz, DMSO, ppm) 12.6 (s, 2H), 7.67 (dd, 2H, $J = 4.2$ Hz), 7.29 (d, 2H), 7.18 (d, 2H,), 2.05 (s, 4H, CH_2); element. anal. (%), found C 52.60; H 3.50; S 26.18; Calc. C 53.73; H 3.32; S 26.39; O 17.56; UV–vis λ_{max}(DMSO) 334 nm (ε 35,000).

2.1.1. Lig. 1-Phen

Erbium trichloride (0.061 mmol, 16.8 mg), 1,10-phenanthroline (0.12 mmol, 22.4 mg) and {4′-(hydroxycarbonyl)methyl-[2,2′;5′,2″]terthiophen-3′-yl}acetic sodium salt (0.12 mmol,
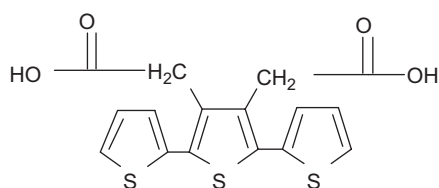
Lig. 1
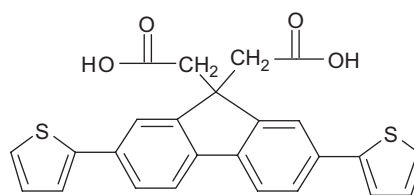
Lig. 2

Fig. 1. Chemical structure of the ligands.

49.9 mg) were dissolved in 20 ml of dry methanol. The cloudy solution was refluxed for 24 h. Meanwhile it turned from pale yellow to pink, producing a precipitate. The solid was isolated by vacuum filtration and dried in vacuum at room temperature, yielding 27.8 mg of a pink solid.

IR (cm^{-1}): FTIR (KBr) 2924(w); 1577(s); 1401(s); 843(m).

Matrix-assisted laser desorption ionization (MALDI)-TOF m/z 1345.7 $C_{57}H_{44}N_4O_9S_6ClErNa$.

UV–vis λ_{max} (DMSO solution) 335 nm.

2.2. 2,7-Dibromo-9,9-bis[(methoxycarbonyl)methyl]-fluorene (A)

2,7-Dibromofluorene (101.2 mg, 0.3 mmol) in anhydrous THF (2.5 ml) was added dropwise at $-78\,^{\circ}$C to the lithium diisopropylamide solution (LDA 0.7 mmol) previously prepared and stirred for 30 min at this temperature. The solution became yellow. Methyl bromoacetate (188.8 mg, 1.23 mmol) was added to the mixture. The solution was allowed to warm to room temperature and stirred for 12 h. The mixture was extracted with diethyl ether and the organic extracts were washed with brine and dried over magnesium sulphate. The solvent was removed and the residue was purified by flash chromatography (hexane: ethyl acetate 8:2) to provide 75.2 mg (yield 53.6%) of the title product as a white solid. MP 187–190 $^{\circ}$C.

^{1}H NMR (270 MHz, CDCl$_3$, ppm) 7.66 (d, 2H, $J = 1.5$ Hz); 7.54 (d, 2H, 8.1 Hz); 7.5 (dd, 2H, $J = 8$ Hz and e $J = 1.5$ Hz); 3.55 (s, 6H); 3.04 (s, 4H).

FTIR (KBr) 2949(w); 1736(s); 1451(m); 1438(m); 1395 (m); 1359 (m); 1272(w); 1248(w); 1197(s); 1159(s); 1066(w); 1005(w); 886(m); 823(s).

UV–vis λ_{max} (THF solution) 281 nm.

2.3. 2,7-(2-Thienyl)-9,9-bis[(methoxycarbonyl)methyl]-fluorene (B)

2,7-Dibromo-9,9-bis[(methoxycarbonyl)methyl]-fluorene (207 mg, 0.44 mmol) and Pd(PPh$_3$)$_4$ (10 mg, 0.009 mmol) were dissolved in 3 ml of dry DMF. After the addition of 2-tributylstannylthiophene (300 mg, 0.94 mmol) the solution was heated at 55 $^{\circ}$C for 1 h and at 105 $^{\circ}$C overnight. The crude solid resulting from solvent removal was purified by flash chromatography using dichloromethane and subsequent recrystallization from heptane, to provide 134 mg of the title compound as a white solid (yield 64%).

MP 123–125 $^{\circ}$C; MS (EI): m/z 474 [M$^+$].

FTIR (cm^{-1}) 2942(w); 1729(s); 1471(w); 1436(w); 1327(m); 1259(m); 1165(s); 810(s).

^{1}H-NMR (400 MHz, CDCl$_3$, ppm) 7.78 (s, 2H), 7.71 (d, 2H, $J = 7.9$), 7.63 (d, 2H, $J = 7.9$), 7.35(d, 2H, $J = 3.2$), 7.28 (d, 2H, $J = 4.9$), 7.09 (dd, 2H, $J = 3.2$ and $J = 4.9$), 3.57 (s, 6H), 3.14 (s, 4H).

UV–vis λ_{max} (DMSO) 352 nm.

2.4. Preparation of the acid (Lig. 2)

Under nitrogen atmosphere, 2,7-di(2-thienyl)-9,9-bis[(methoxycarbonyl)methyl]-fluorene (121 mg, 0.25 mmol) was dissolved in 2.5 ml of THF dry and refluxed with a solution of sodium hydroxide (5–10 wt%) in 2.5 ml of methanol. As the hydrolysis went on, the solution became opaque, then a considerable amount of insoluble solid appeared after 24 h. The reaction was allowed to proceed for another 2 days, monitoring it by TLC (eluent CH$_2$Cl$_2$). Then, the mixture was poured into 100 mL of distilled water under vigorous stirring to form a milky solution. After acidification with diluted hydrochloric acid (0.5 M), the resulting white material was isolated by filtration and washed thoroughly with doubly distilled water. The resulting acid was dried in vacuum for 24 h (yield 69%).

MP 232–234 $^{\circ}$C; FTIR (cm^{-1}) 3067(w), 1708(s), 1469(m), 1420(m), 1207(m), 854(s), 692(s).

^{1}H-NMR (500 MHz, CD$_3$OD, ppm) 7.88 (s, 2H), 7,67 (d, 2H, $J = 7.9$), 7.57 (d, H, $J = 7.9$), 7.36 (d, 2H, $J = 3.2$), 7.35 (d, 2H, $J = 4.9$), 7.04 (dd, 2H, $J = 3.2$ and $J = 4.9$), 3.10 (s, 4H). The acid proton disappeared after exchange with deuterated methanol; element. anal. (%), found C 67.15; H 4.22; S 14.08; calc. C 67.24; H 4.06; S 14.36; O 14.33.

UV–vis λ_{max} (DMSO) 352 nm (ε 50,000).

2.4.1. Lig. 2-Phen

Under nitrogen atmosphere, triethylamine freshly distilled (0.04 ml, 0.28 mmol) was added by syringe to a solution of **Lig. 2** (63 mg, 0.14 mmol) in reagent grade MeOH (5 ml) in order to assure its dissolution. 20.8 mg of ErCl$_3$ was dissolved in 2 ml of MeOH and added to the previously prepared solution. A reaction took place immediately, and a white viscous solid appeared, and the reaction mixture was stirred for half an hour. A precise amount of 1,10-phenanthroline (26.7 mg, 0.15 mmol) was dissolved in 2 mL of MeOH and added by a syringe to the mixture. The reaction mixture was refluxed under stirring overnight. After cooling, a pink precipitate was isolated by vacuum filtration to provide 67 mg of a complex, which results to be hygroscopic.

UV–vis λ_{max} (MeOH) 355 nm, small intensity peaks at 480, 520, 670 nm due to Er^{3+}.

FTIR (cm^{-1}) 3067(w), 1556(s), 1468(m), 1424(s), 814(s), 696(m).

MALDI and electron spray injection (ESI): complex decomposition occurs.

SEM Er/S = 1/4, elemental analysis for ErS$_4$O$_9$N$_2$ C$_{62}$H$_{41}$ $\cdot$ 3H$_2$O, found: C 56.22; H 3.22; N 2.07; S 9.59; calc: C 56.96; H 3.69; N 2.14; S 9.80.

2.5. Apparatus

^{1}H (270, 400, and 500 MHz) spectra were measured with Bruker and Bruker Advance instruments, respectively. Gas chromatograms were performed using an Agilent Network

GC System 6890N instrument. Melting points were determined by using a Mettler PF5 instrument. Electron-impact mass spectrometry measurements were performed on a VG ZAB-2F spectrometer equipped with a FI/FD ion source kept at ca. 200 °C operating at 8 kV accelerating and 4 kV output potentials and with the emitter activated according to the standard VG micromass procedure.

MALDI mass spectra were obtained by an Ultraflex II mass spectrometer (Bruker Daltonics) operating both in the positive reflectron and in the linear modes, using 2,5-dihydroxybenzoic acid as the matrix.

ESI mass spectra were carried out using a MicrOTOF Bruker apparatus.

The morphology, homogeneity and the metal/sulphur ratio of the complexes were investigated by using a Philips XL40 model scanning electron microscope (SEM) equipped with an EDAX DX PRIME X-ray energy dispersive spectrometer (EDS) [21].

FTIR spectra were recorded on a Bruker IFS 48 instrument, using KBr pellets. FTIR spectra of films were taken in the reflection–absorption mode. Electronic spectra were obtained from a Lambda 900 Perkin-Elmer spectrometer.

NIR and UV/vis PL measurements have been carried out by exciting the complexes in anhydrous dilute solution of DMSO with the III harmonic of a pulsed Nd:YAG laser focused with a cylindrical lens to reduce the sample heating/degradation (power 0.5 mW, repetition rate 10 kHz, pulse duration 10 ns). The signal, dispersed with a monochromator (15 and 3 nm bandwidth in the IR and UV/vis regions, respectively), has been detected with a Hamamatsu R5509-73 photomultiplier and recorded in the photon counting mode with a Ortec 9353 multichannel scaler. The overall time resolution was better than 30 ns.

3. Results and discussion

3.1. Preparation of the complexes

The complexes are based on the coordination to Er^{3+} of two carboxyl (COO^-) groups which are substituents of aromatic rings acting as sensitizers in the energy-transfer process from the visible to the IR region. we have considered two different aromatic moieties, namely a thiophene ring in which the carboxyl functionalities are attached to adjacent carbon atoms, and a fluorene one where the carboxyls are substituents on the same carbon atom. Two additional thiophene rings terminate the antenna ligands **Lig. 1** and **2** as shown in Fig. 1.

Lig. 1 has been prepared as reported in Ref. [12], while **Lig. 2** has been obtained through a Stille coupling mediated by Pd(0)tetrakis of 2,7-dibromo-9,9-bis[(methoxycarbonyl)methyl]-fluorene with 2-tributylstannylthiophene followed by a hydrolysis of the ester group yielding the di-acid compound. ^{1}H NMR, FTIR and UV–vis spectroscopies carried out on **Lig. 2** are in agreement with the structure proposed in Fig. 1. Indeed, NMR spectrum of **Lig. 2**

carried out in CD_3OD shows the disappearance of the singlet due to hydrogen atoms of the methoxy group at 3.57 ppm in $CDCl_3$, and a shift of the methylene proton signal from 3.14 to 3.10 ppm. At 12.6 ppm, the acid proton of the hydroxycarbonyl functionality remaining after the hydrogen–deuterium exchange with the solvent clearly appears. The complexation of the two ligands carrying pyridine or 1,10-phenanthroline as ancillary ligands (**L**) follows the scheme reported below.

$2\textbf{Lig}$ (acid or salt form) $+ ErCl_3 + nL \rightarrow (Lig)_2 \ ErX \ L_n$.
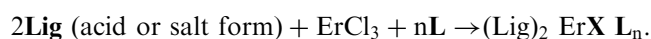
Lig = **Lig. 1**. When starting from the acid, it is necessary to previously obtain the salt by adding $NaOCH_3$
 = **Lig. 2**. The salt is obtained "in situ" using NEt_3 as a base.
X = Na^+ or Cl^- or OH^- counter ion.

Lig. 1 sensitized complexes have been prepared with both ancillary ligands, while for **Lig. 2** only phenanthroline has been used. Unfortunately no crystals suitable for XRD analysis have been obtained, hence the constitutional formulae have only been derived using MALDI and ESI. **Lig. 1-Py** is a mixture of mono-metal molecule and dimeric species in different ratios, and the stability of this complex has been confirmed by using the ESI analysis, by which the whole molecule can be observed. On the contrary, **Lig. 1-Phen** is a well-defined species, where just one clamp of each antenna molecule is coordinated to the lanthanide metal using both oxygen atoms of the carboxyl function. The molecular weight of **Lig. 2-Phen** could not be determined by MALDI or ESI, possibly due to a lack of stability during analysis, while a SEM investigation indicated an erbium to ligand ratio of 1:2, and elemental analysis of the organic fraction revealed the presence of coordinated water molecules.

On the basis of the above considerations the chemical structure of **Lig. 1-Py** can be sketched as in Scheme 1, while Scheme 2 shows the constitutional formula of the **Lig. 1-Phen** and **Lig. 2-Phen** complexes.

3.2. Spectroscopical characterization

UV–vis and FTIR investigations have been performed on ligands and complexes. DMSO, a solvent where also the complexes can dissolve, has been employed for the former analysis, while the latter characterization has been carried out using KBr pellets. The absorption spectra will be discussed below in comparison with the theoretical data

Scheme 1.

Lig.1-Phen   Lig.2-Phen
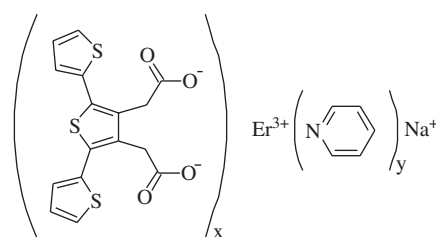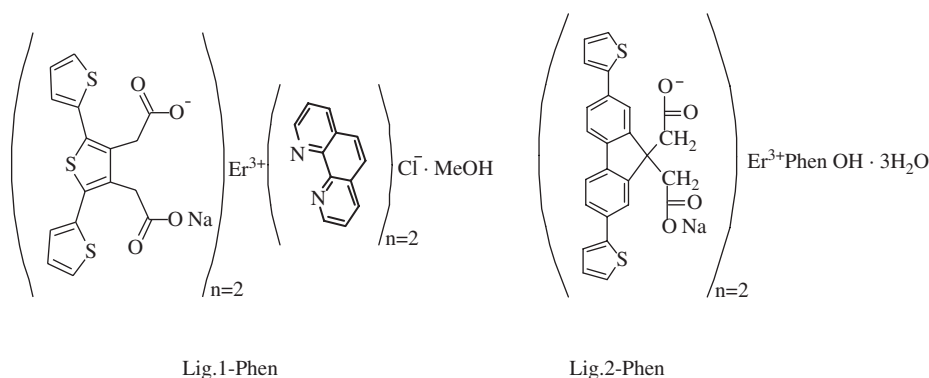
Scheme 2.

obtained from quantum chemical calculations. For the moment, we only outline here that the maximum in the absorption spectrum of the acidic form of **Lig. 1** in DMSO is centred at 334 nm (ε 35,000), while the maximum of the spectrum of protonated **Lig. 2** is observed at 352 nm (ε 50,000).

The FTIR spectrum of the acidic form of **Lig. 1**, reported in Fig. 2, shows a peak at 1696 cm^{-1} (to be obviously associated with the dimeric form of the acid), which disappears upon complexation. In the spectrum of **Lig. 1-Py** two bands appear at 1741 and 1465 cm^{-1} which can be attributed to the antisymmetric (v_{as}) and symmetric (v_s) vibrational modes of carboxylate moieties, respectively [13,14]. On the contrary, for the complex **Lig. 1-Phen** (see Fig. 3), both vibrations originate bands shifted towards lower frequencies with respect to the $C=O$ band of **Lig. 1**. All these data are collected in Table 1, where the frequencies of **Lig. 2** as well as those of **Lig. 2-Phen** are given. Note that also for the more encumbered phenantroline co-ligand, an even more pronounced shift towards lower energies is observed for both antisymmetric and symmetric stretchings.

The position of the peaks related to the v_s (COO^-) mode is approximate because of their broadening (see Fig. 2) due to the overlap with the signals of phenantroline, $C=C-C$ bending of thiophene, and CH_2 bending of side clamps. However, it is pleasing to see that there is a substantial agreement between our findings and those reported by other authors [13,14] for fatty acids.

According to these authors, the peak positions of antisymmetric and symmetric vibrational modes of carboxylate as well as their shift with respect to the frequency of the acidic $C=O$ strongly depend on the metal ion–carboxylate coordination. The three possible types of coordination are sketched in Fig. 3.

In agreement with the discussion in Refs. [14,15], the FTIR data of **Lig1-Py** are consistent with a monodentate coordination, as shown in Fig. 3(a) no equivalence of CO bonds is present, and an increase in v_{as} and a decrease in v_s with respect to the above-mentioned acidic CO stretching are observed. The frequency separations Δ observed in the
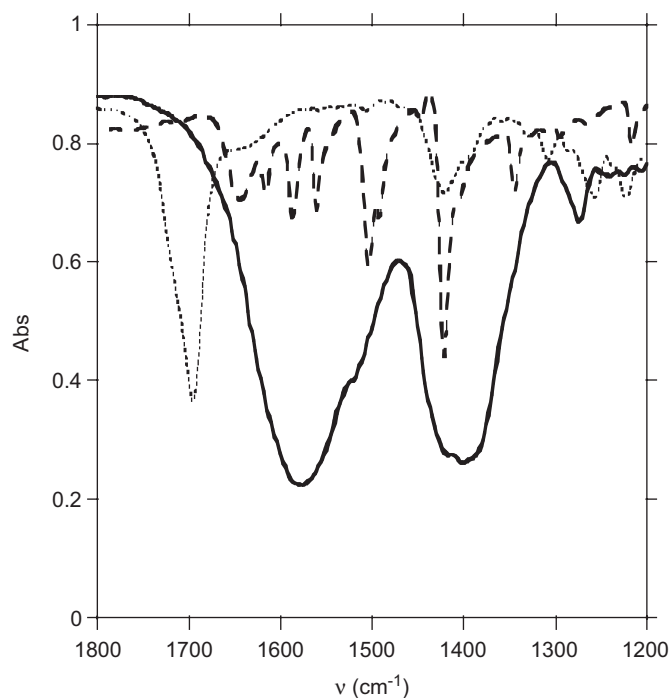

Fig. 2. FTIR spectra of **Lig. 1** acid (dotted line), phenantholine (broken line) and Er**Lig. 1**-Phen (full line) (see the text).
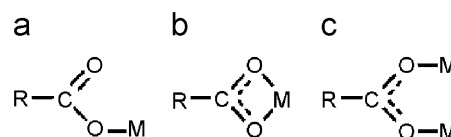

Fig. 3. Schematic representation of the main types of metal-carboxylate coordination. (a) monodentate; (b) chelating bidentate and (c) bridging bidentate.

Lig. 1-Phen and **Lig. 2-Phen** complexes are consistent with a chelating bidentate coordination, both being smaller than 150 cm^{-1} (see Ref. [15]). On the other hand, sterical hindrance in the complex is expected to work against a bridging bidentate coordination.

In this view, the spatial structures of the three complexes are sketched in Fig. 4.

Table 1
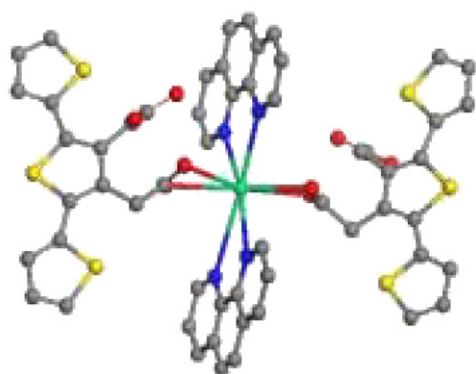Frequencies (cm^{-1}) of the C=O antisymmetric stretching modes of ligands (acidic form) and COO$^-$ antisymmetric and symmetric stretching modes of Er-complexes together with their frequency separations
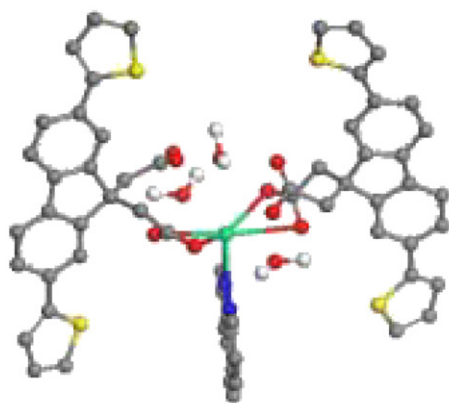
Compound	ν_{as} (C=O)	ν_{as} (COO)	ν_s (COO)	$\Delta = \nu_{as} - \nu_s$
Lig. 1	1696			
Lig. 1-Py		1741		276
			1465	
Lig. 1-Phen		1577		146
			1431	
Lig. 2	1704			
Lig. 2-Phen		1556		131
			1425	
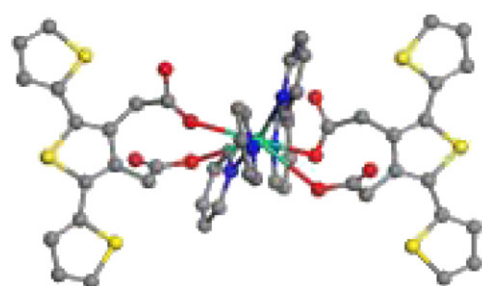
Lig.1-Py

Lig.1-Phen

Lig.2-Phen

Fig. 4. Spatial structures of the complexes considered in this work.

3.3. PL

Steady-state and time resolved fluorescence emission spectra in the NIR spectral region have been measured for the Er^{3+} complexes in DMSO anhydrous solutions. Upon excitation in the ligand absorption band, all the samples show an intense emission at 1.5 μm due to the Er^{3+} $^4I_{13/2}$–$^4I_{15/2}$ transition confirming the formation of the complexes and the occurrence of an effective energy transfer from the ligand excited states towards the Er^{3+} ones. In particular, Fig. 5 displays the absorption of **Lig. 1**, its visible emissions of both singlet and triplet states, this latter being detectable only at 77 K, together with the intense NIR emission of lanthanide ion. The PL quantum yield (QY) can be evaluated by comparison with the emission of the [ErQ$_3$] (Q = 8-hydroxyquinolinate), recorded in the same experimental conditions. This complex can be considered the actual benchmark for this class of IR emitters, with an emission efficiency of a few units × 10^{-4} upon both optical and electrical excitation [16,17]. As reported in Table 2, the efficiencies of all our complexes are of the same order of magnitude, with **Lig. 1-Py** matching the performance of ErQ$_3$.

Time-resolved PL measurements give deeper insight on the processes involved in the IR emission. As shown in the inset of Fig. 5 for **Lig. 1-Phen**, the 1.5 μm PL decay follows a perfect single-exponential law, suggesting that Er^{3+} experiences the same mean local environment. Similar results are obtained for the **Lig. 1-Py** complex, while the poor stability of **Lig. 2-Phen** strongly affects PL decay measurements, making the data obtained for this last complex less reliable. The observed decay times are around 2 μs (Table 2). In organolanthanide complexes, in which the excitation is funnelled to the rare earth via energy transfer from the ligand, the overall QY is given by the products of two factors: the yield of the energy transfer process and the PL QY of the excited Er^{3+} ions. This latter term is strictly related to PL decay rate being the Er^{3+} emission QY determined by the rate at which radiative and non-radiative processes depopulate the excited states (k_{rad} and $k_{non\text{-}rad}$, respectively). The fraction of ions, which decay through light emission, is given by $k_{rad}/(k_{rad} + k_{non\text{-}rad})$. The Er^{3+} $^4I_{13/2}$–$^4I_{15/2}$ transition is parity forbidden. Of consequence its radiative decay time (τ_{rad}) is very slow being about 15 m/s regardless of the host material in which Er^{3+} is contained. The corresponding $k_{rad} = 1/\tau_{rad}$ is around 10^2 Hz. On the contrary, the total decay rate ($k_{rad} + k_{non\text{-}rad}$) depends on the average time the ions spend in the excited states prior to returning to their ground state and determines the observed PL decay time $1/\tau = (k_{rad} + k_{non\text{-}rad}) \cong 10^6$ Hz. These data imply that in our complexes the emission efficiency of the Er^{3+} ions must be in the range of 10^{-4} as experimentally measured for the total QY. Therefore, the factor limiting the efficiency of the complexes is, as usual, the presence of nonradiative decay channels enhancing the natural decay rate of the Er^{3+} $^4I_{13/2}$ excited state, while the transfer
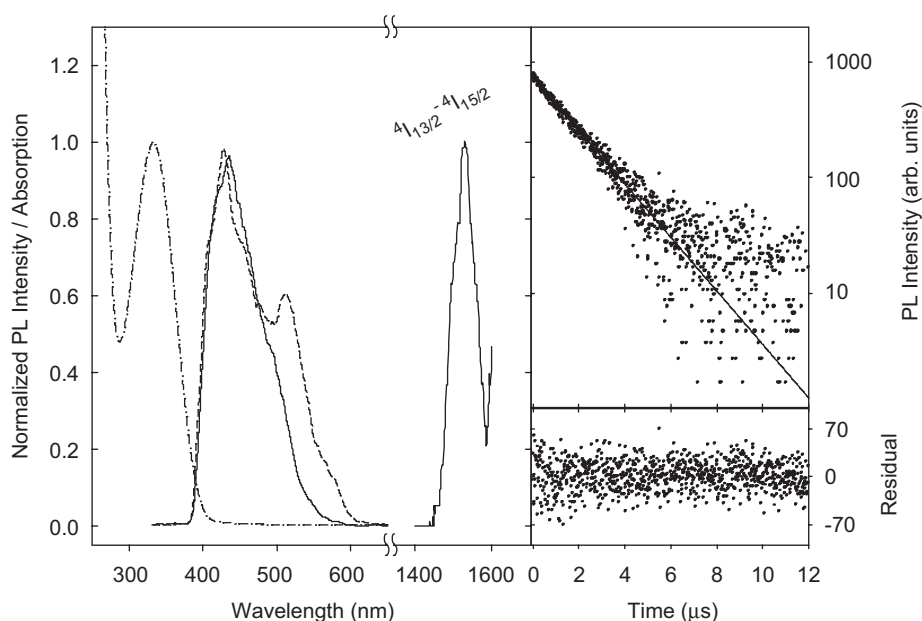
Fig. 5. Absorption and visible emission (solid line at 298 K, dashed line at 77 K) and NIR emission spectra of **Lig. 1-Phen** complex in DMSO solution excited at 355 nm. In the right panel the erbium $^4I_{13/2}$–$^4I_{15/2}$ PL decay is reported.

Table 2
Photoemission parameters

Complex	Lifetime (μs)	Relative total efficiency (%)	Relative transfer efficiency (%)
ErQ$_3$	1.8	100	100
Lig. 1-Py	2.1	100	86
Lig. 1-Phen	1.9	25	24
Lig. 2-Phen	—	30	—

efficiencies (TE) from the ligands are expected to be very high. Assuming that the differences between the Er^{3+} radiative decay rate are negligible in the set of investigated complexes, the TE relative values can be easily obtained from the lifetime and relative QY measurements as TE $\propto$ QY/τ. In Table 2, lifetime, QY and TE data (the latter two normalized at the corresponding values in ErQ$_3$) are summarized.

It is evident that in the newly sensitized complexes the transfer efficiency is less than in ErQ$_3$, while the corresponding PL lifetimes are slightly slower. The quenching in the Er complexes is mainly due to back-transfer to the overtone of the ligand C–H vibrational modes, which are nearly resonant with the $^4I_{13/2}$–$^4I_{15/2}$ transition. Since both the Er^{3+} excitation and quenching are controlled by energy transfer processes depending on the donor–acceptor distance, these data suggest, in agreement with the complex models in Fig. 4, that in our organometal compounds the mean distance Er-ligand is slightly longer than in ErQ$_3$. In fact, in the latter the quinolinate moiety is directly bonded to the metal, while in the complexes reported here the antenna is indirectly linked (through at least three bonds).

It is worth remarking that the above considerations cannot be considered as exhaustive, due to the difficulties in evaluating the dissociation constants of the complex in DMSO solution, which affect the transfer efficiency. In order to avoid the coordination of DMSO the emission measurements were carried out immediately after solution preparation. However, these arguments are in favour of the trend of Table 2, which otherwise would be hardly justified by the effective matching between a triplet state of the organic sensitizer and the excited $^2H_{11/2}$ erbium level [18].

3.4. Quantum chemical calculations

We have studied the geometry and the electronic properties of each *isolated* ligand through quantum chemical methods. Due to the mainly electrostatic nature of the interaction between the coordinating atom and the ligands, it may be argued that the two carboxyl moieties occurring in each ligand will enter the complex in their deprotonated form. Anyway, in every case we have studied both the acid (neutral) and the doubly deprotonated (dianion) forms of each ligand.

Theoretical geometries have been obtained through geometry optimizations carried out by using the semiempirical PM3 hamiltonian without imposing any symmetry constraint, and they have been compared with the observed ones in the crystal structure of the quinquithiophene homologous [19]. Although the geometry details will be described in a forthcoming paper, a few short comments are in order here. For both ligands some C$_2$ symmetry emerges from the calculations, and there are no appreciable differences in bond lengths and angles between the neutral and dianion forms. Due probably to steric hindrance, for neutral **Lig. 1**, the substitution enhances the non-planarity,

which is already present in unsubstituted terthiophene [20]. The two $C{=}O$ bonds lie in an *anti* position with respect to the plane of the central thienyl, although the situation could become different when the ligand enters the complex, as will be shown below. The **Lig. 2** molecule consists of three separately conjugate sections, namely the central condensed system and the two side thienyl rings, whose planes are somewhat rotated with respect to the latter. For both ligands the neutral and the dianion forms, although being *isoelectronic*, show markedly different molecular orbitals, this being true in particular for the HOMO's and the LUMO's. In neutral **Lig. 1** both the latter orbitals are spread over the same two adjacent thienyl rings, while in the dianion the HOMO extends over the central thienyl and its substituents, and the LUMO over all three thienyls. In neutral **Lig. 2** both frontier orbitals cover the central condensed system, while in the dianion the HOMO extends over the carboxyl groups only (with small tails on the condensed system), and the LUMO on the side thienyls.

The lowest singlet and triplet transitions have been computed through full configuration interaction on singles (CIS) semiempirical INDO calculations, and Figs. 6 and 7 display the predicted spectra for the neutral and deprotonated forms of **Lig. 1** and **Lig. 2,** respectively (together with the experimental absorption spectra of the complexes), while the positions of the singlet and triplet transitions are reported in Table 3.

The spectra of the two forms of **Lig. 1** differ strongly, and in particular the most intense peak (at 341 nm) of the spectrum of the neutral form is in an even surprising agreement with the corresponding experimental results for

Fig. 6. Experimental absorption spectra of **Lig. 1-Py** and **Lig. 1-Phen** complexes, and CIS-INDO optical spectra for neutral and dianionic **Lig. 1**. Each spectrum is normalized to its highest absorption peak, and the stick spectra are proportional to the oscillator strengths.
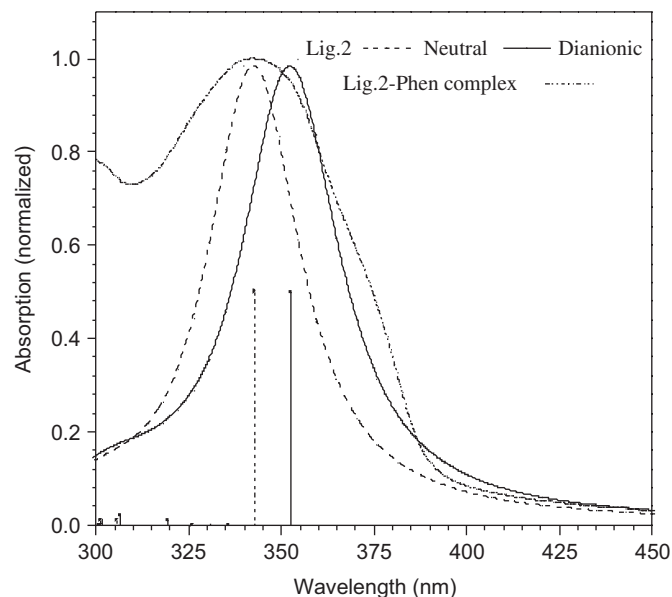

Fig. 7. Experimental absorption spectrum of the **Lig. 2-Phen** complex and CIS-INDO optical spectra for neutral and dianionic **Lig. 2**. Each spectrum is normalized to its highest absorption peak, and the stick spectra are proportional to the oscillator strengths.

Table 3
Lowest CIS-INDO[a] singlet and triplet transitions ordered by excitation energy (cm^{-1}), and the corresponding λ (nm) and oscillator strengths for the neutral and dianionic forms of **Lig. 1** and **2**

Exc.	Neutral			Dianionic		
	Energy	λ	f	Energy	λ	f
Lig. 1						
T_1	18,483.0	541.0	—	15,159.3	659.7	—
T_2	21,209.0	471.5	—	19,263.6	519.1	—
T_3	21,272.5	470.1	—	23,567.4	424.3	—
S_1	29,293.2	341.4	0.524	23,974.9	417.1	0.722
T_4	29,618.5	337.6	—	28,605.1	349.6	—
S_2	34,531.2	289.6	0.106	29,313.0	341.1	0.181
S_3	35,335.6	283.0	0.129	39,113.3	255.7	0.046
S_4	47,612.2	210.0	0.296	46,837.0	213.5	0.016
Lig. 2						
T_1	19,898.5	502.5	—	20,094.2	497.7	—
T_2	20,500.3	487.8	—	20,519.4	487.3	—
T_3	25,332.6	394.7	—	25,481.5	392.4	—
S_1	29,179.1	342.7	1.493	28,363.8	352.6	1.300
T_4	30,012.3	333.2	—	29,769.0	335.9	—
S_2	43,366.4	230.6	0.549	39,422.7	253.7	0.204
S_3	47,063.8	212.5	0.416	44,746.6	223.5	0.216
S_4	47,522.4	210.4	0.510	44,972.4	222.4	0.278

[a]Using the full active space.

the complexes including, besides **Lig. 1**, pyridine (335 nm) or phenanthroline (340 nm). On the contrary, the most intense peak of the spectrum of the dianion form (at 417 nm) has absolutely no experimental counterpart. A trivial, albeit highly questionable, explanation of this could be that the ligand form in the complex is not the dianion, but rather the neutral one. Alternatively, this
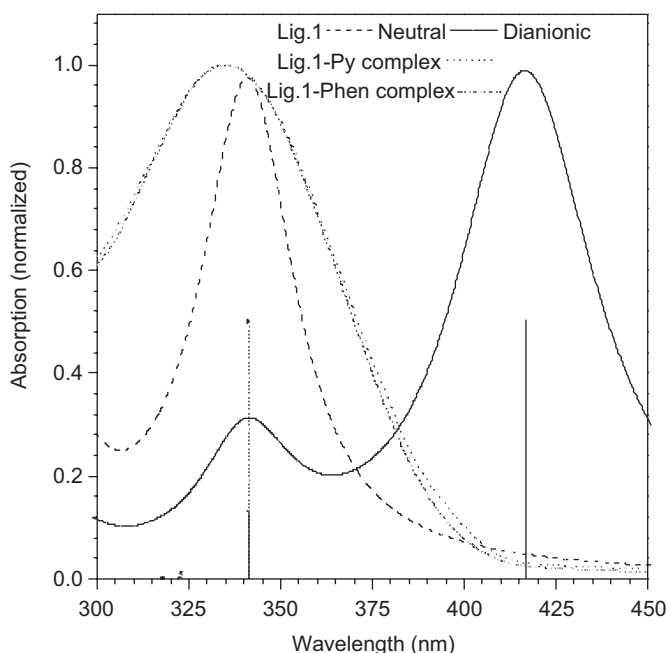
discrepancy could cast doubts on the ability of the present approach to adequately describe the transitions of the dianion form, possibly in relation to the well-known basis set problems that can occur in such systems. That this should not be the case, however, is shown by the theoretical spectra of Fig. 7, which refer to the neutral and dianion forms of **Lig. 2**, and both exhibit a close resemblance between each other, as could have been expected on the basis of the very nature of the carboxyl moiety. On the other hand, the main peaks of the neutral and dianion forms (at 343 and 353 nm, respectively) nicely match the corresponding experimental result for the **Lig. 2** complex containing phenanthroline (at 354 nm). The discrepancy referred to above must then be traced back to some different origin, which is unique to **Lig. 1** and does not hold for **Lig. 2**. In this respect, it can be recalled that an essential difference between the object of our dianion calculations and the experimental complex is the absence of any counter ion in our case. We have overcome this limitation by simply admitting, besides the dianion, the presence of a univalent (Na^+) or of a divalent (Zn^{2+}) positive ion, the geometry of the whole system—including the position in space of the counter ion—being reoptimized using the same PM3 hamiltonian. The predicted spectra of the **Lig. 1** dianion in the presence of a univalent or of a divalent counter ion are reported in Fig. 8. It is apparent that the counter ion causes a strong blueshift (down to 379 nm with Na^+) of the main peak (and of the whole spectrum), and that a further although less, blueshift (down to 356 nm with Zn^{2+}) is determined by its charge increase, so that the spectrum of the (**Lig. 1** dianion plus the divalent counter ion) system becomes essentially similar to that of the neutral form and to the experimental spectrum of the complex, as was the case of **Lig. 2**. The effect of the counter

ions can be simply explained as follows. In **Lig. 1** the carboxyl moieties can move widely, and it can be easily seen that in the isolated dianion a strong interaction gets established between a negatively charged oxygen of one carboxyl and a close hydrogen atom belonging to one of the side thienyls, and the same happens for the second carboxyl and thienyl moieties. In these conditions, terthiophene tends to become planar, which in turn implies a strong red-shift in the dianion absorption with respect to that of the neutral form. Note that nothing similar can happen with **Lig. 2**, where the very rigid structure of the central condensed system constrains the carboxyl moieties to remain very far from the thienyl hydrogen atoms, thus preventing the formation of any hydrogen bond. When we explicitly admit a positive counter ion in addition to the **Lig. 1** dianion (a situation which in some way mimics the actual one in the complex), electrostatic interaction with the net charge overwhelms the interaction with the only partially charged thienyl hydrogen atoms. In fact, the counter ion settles in a central placement, the two $C=O$ bonds move (in the divalent case) to a *syn* position with respect to the plane of the central thienyl, and the conjugation in tertiophene drops, giving rise to a substantial blueshift in the electronic spectrum.

The univalent/divalent counter ion can model in some way the coordinating ion bonded to phenanthroline/ pyridine, and in this respect the univalent→divalent theoretical shift in the wavelength of the strongest peak results to be in the right direction, although the amount of the experimental shift is much less. This is due, among others, to the fact that the actual complex is a much more crowded system than is its model (ligand plus counter ion) one, and accordingly in the latter the interactions, as well as their variations, can be markedly stronger, occurring between closer subjects. Finally, the possibility of varying the main peak of the spectrum in relation to the charge of the coordinating atom appears to be an attractive property of the **Lig. 1** ligand.

Adding a counter ion to the **Lig. 1** dianion has an even bigger effect on the triplet transitions (the results of INDO/ CIS calculations on a basis of 50 occupied/50 virtual orbitals are reported in Table 4), and in particular the lowest forbidden transition T_1 blueshifts down to 554 nm, i.e. by more than 100 nm, in the presence of a divalent
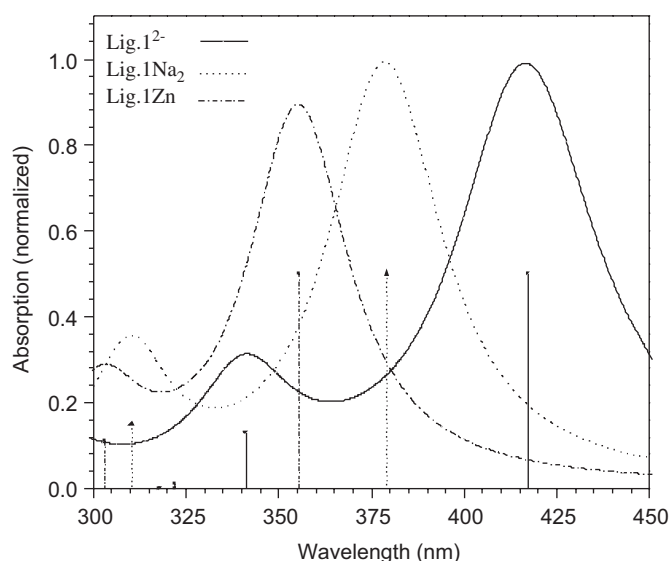

Fig. 8. CIS-INDO optical spectra for the **Lig. 1** dianion both isolated and in the presence of a Na^+ or a Zn^{2+} counter ion. Each spectrum is normalized to its highest absorption peak, and the stick spectra are proportional to the oscillator strengths.

Table 4
Lowest CIS-INDO[a] triplet excitation energies (cm^{-1}) and λ (nm) for the isolated **Lig. 1** dianion (L_1^{2-}), the sodium (L_1Na_2) and the zinc (L_1Zn) salt

Exc.	L_1^{2-}		L_1Na_2		L_1Zn	
	Energy	λ	Energy	λ (nm)	Energy	λ
1	15,159.3	659.7	16,516.9	605.4	18,045.0	554.2
2	19,263.6	519.1	20,349.5	491.4	20,691.6	483.3
3	23,567.4	424.3	22,865.5	437.3	21,834.4	458.0
4	28,605.1	349.6	29,267.5	341.7	29,374.5	340.4

[a]Using an active space of 50 occupied and 50 virtual orbitals.

counter ion. A further shift towards higher energy is expected for the lanthanide 3^+ ion. In fact low-temperature measurements show **Lig. 1** triplet emission at 518 nm (see Fig. 5). Reasoning as above, this is seen to effect the theoretical emission properties of the two **Lig. 1** complexes, in that the erbium–pyridine complex is predicted to be more efficient than the erbium–phenanthroline one [$\lambda(T_1) = 605$ nm], the erbium $^4I_{15/2} \rightarrow {}^2H_{11/2}$ transition lying at about 520 nm.

4. Conclusions

Three erbium complexes carrying thiophene (**Lig. 1**) and thiophene–fluorene (**Lig. 2**) moieties as antennae have been synthesized and characterized. **Lig. 1** complexes result to be stable whatever the ancillary ligand, as proved by mass spectrometry determinations. Because of the poor stability of **Lig. 2-Phen**, MALDI could not provide a unique chemical structure for this complex. However, by combining MALDI and SEM-FTP techniques, a reliable stoichiometry for all materials has been obtained. Detailed FTIR analyses allow to distinguish among the Er-sensitizer coordination types, namely monodentate for **Lig. 1-Py** and chelating bidentate for **Lig. 1-Phen** and **Lig. 2-Phen**. Quantum chemical calculations have been carried out in order to explain optical absorption data also in relation to the coordination type. We have studied the geometry, the electronic spectrum and the lowest triplet transitions of the neutral and doubly deprotonated forms of each isolated ligand. In the dianion case the complexes containing phenanthroline/pyridine are modelled by adding one univalent/divalent counterion. For both ligands the computed absorption spectra of the dianions in the presence of a divalent counterion are found to be in close agreement with experiment, and the univalent→divalent theoretical shift in the wavelength of the strongest absorption peak results to be in the right direction. The possibility of varying the position of the main peak of the spectrum in relation to the charge of the coordinating atom appears to be an attractive property of **Lig. 1**. Moreover, NIR emission data in the 1400–1600 nm range are explained in terms of the three processes involved in the overall Er^{3+} emission, namely energy transfer from the sensitizer to metal, emission of the rare earth after thermalization, and quenching. Time resolved measurements indicate that energy transfer efficiencies are in the order $ErQ_3 >$ **Lig. 1-Py** > **Lig. 1-Phen**, which parallels the increase in the Er-sensitizer distance. Moreover, theoretical emission properties predict the erbium–pyridine complex to be more efficient than the erbium–phenanthroline one, because of a more effective matching between a triplet state of the sensitizer and the $^2H_{11/2}$ erbium level. Such a matching may be considered as an important requirement for the design of highly luminescent lanthanide materials.

Acknowledgements

References

[1] A. Polman, J. Appl. Phys. 82 (1997) 1.

[2] L.H. Slooff, A. Van Blaaderen, A. Polman, G.A. Hebbink, S.I. Klink, F.C.J.M. van Veggel, D.N. Reinhoudt, J.W. Hofstraat, J. Appl. Phys. 91 (2002) 3955.

[3] N. Sabbatini, M. Guardigli, J.-M. Lehn, Coord. Chem. Rev. 123 (1993) 201.

[4] N.M. Shavaleev, S.J.A. Pope, Z.R. Bell, S. Faulkner, M.D. Ward, J. Chem. Soc., Dalton Trans. 1 (2003) 808.

[5] L.H. Slooff, A. Polman, F. Cacialli, R.H. Friend, G.A. Hebbink, F.C.J.M. van Veggel, D.N. Reinhoudt, Appl. Phys. Lett. 78 (2001) 2122.

[6] M.H.V. Werts, J.W. Verboeven, J.W. Hofstraat, J. Chem. Soc., Perkin Trans. 2 (2000) 433.

[7] Y. Korovin, N. Rusakova, J. Fluoresc. 12 (2002) 159.

[8] L.H. Slooff, A. Polman, S.I. Klink, G.A. Hebbink, L. Grave, F.C.J.M. van Veggel, D.N. Reinhoudt, J.W. Hofstraat, Opt. Mater. 14 (2000) 101.

[9] G.E. Buono-Core, H. Li, B. Marciniak, Coord. Chem. Rev. 99 (1990) 55.

[10] S. Destri, W. Porzio, F. Meinardi, R. Tubino, G. Salerno, Macromolecules 36 (2003) 273.

[11] R.M. Osuna, R. Ponce Ortiz, C. Ruiz Delgado Mari, Y. Sakamoto, T. Suzuki, V. Hernandez, J.T. Lopez Navarrete, J. Phys. Chem. B 109 (2005) 20737.

[12] A. Fazio, B. Gabriele, G. Salerno, S. Destri, Tetrahedron 55 (1999) 485.

[13] L. Haolong, B. Weifeng, Q. Wie, W. Lixin, J. Chem. Phys. B 109 (2005) 21669.

[14] E.F. Marques, H.D. Burrows, M. da Graça Miguel, J. Chem. Soc., Faraday Trans. 94 (1998) 1729.

[15] Y. Ren, K. Imura, A. Ogawa, T. Kato, J. Phys. Chem. B 105 (2001) 4305.

[16] R. Pizzoferrato, L. Lagonigro, T. Ziller, A. Di Carlo, R. Paolesse, F. Mandoj, A. Ricci, C. Lo Sterzo, Chem. Phys. 300 (2004) 217.

[17] R.J. Curry, W.P. Gillin, A.P. Knights, R. Gwilliam, Appl. Phys. Lett. 77 (2000) 2271.

[18] M. Ottonelli, G.M.M. Izzo, F. Rizzo, G. Musso, G. Dellepiane, R. Tubino, J. Phys. Chem. B 109 (2005) 19249.

[19] W. Porzio, S. Destri, M. Pasini, U. Giovannella, S.V. Meille, G. Raos, R. Consonni, G. Zotti, Chem. Mater. 17 (2005) 242.

[20] F. Van Bolhuis, H. Wymberg, E.E. Havinga, E.W. Meijer, E.G.J. Staring, Synth. Met. 30 (1989) 381.

[21] P. Guerriero, P.A. Vigato, B. Burtet-Fabris, Inorg. Chim. Acta 164 (1989) 155.